


Article

Analysis and Design of Three-Phase LLC Resonant Converter with Matrix Transformers

Jing-Yuan Lin, Hsuan-Yu Yueh, Yi-Feng Lin *  and Pin-Hsien Liu

Department of Electronic and Computer Engineering, National Taiwan University of Science and Technology, Taipei 10607, Taiwan; jylin@mail.ntust.edu.tw (J.-Y.L.); kyleyueh@gmail.com (H.-Y.Y.); 2016anewera@gmail.com (P.-H.L.)

* Correspondence: d10302013@mail.ntust.edu.tw; Tel.: +886-2-2730-1288

Abstract: This study presents the topology of a three-phase LLC resonant converter with matrix transformers. The three-phase LLC resonant converter has the advantages of conventional LLC resonant converters, including zero-voltage switching at the primary side, zero-current switching at the secondary side, high-frequency feasibility, and high efficiency. Moreover, it has additional advantages that differ from conventional LLC, including low output capacitor current ripple, natural current sharing in three resonant currents, and a high power level. As a result of the above mentioned characteristics, LLC topology has been used in many electric vehicle charging systems, server power systems, and other high-power applications. However, as the power level becomes higher and higher, the input voltage is usually too high to reduce conduction loss, and the output current also increases. This situation makes transformer design more difficult. The increasing current means more core and copper loss, and the heat dissipation of the transformer becomes more difficult. Matrix transformer technology can improve this problem directly and simply. By utilizing matrix transformers, which are primary series connected and secondary parallel connected, the primary voltage stress and secondary current stress of the transformers can be reduced, and the output current can be distributed. The analysis of the proposed converter in this study includes a circuit operation introduction, a time-domain analysis, calculation of the transfer ratio curve in the frequency domain, and a loss analysis. The theoretical analysis and performance of the proposed converter are verified. A three-phase LLC resonant converter with matrix transformers prototype is built with a high input voltage of 800-VDC and high output current of 200-A. The output voltage is 100-VDC. The waveform and efficiency data will be shown in the experimental results.

Keywords: matrix transformers; three-phase Y-Y LLC; LLC converter



Citation: Lin, J.-Y.; Yueh, H.-Y.; Lin, Y.-F.; Liu, P.-H. Analysis and Design of Three-Phase LLC Resonant Converter with Matrix Transformers. *Energies* **2022**, *15*, 1315. <https://doi.org/10.3390/en15041315>

Academic Editors: Md Rasheduzzaman and Teuvo Suntio

Received: 30 December 2021

Accepted: 8 February 2022

Published: 11 February 2022

Publisher's Note: MDPI stays neutral with regard to jurisdictional claims in published maps and institutional affiliations.



Copyright: © 2022 by the authors. Licensee MDPI, Basel, Switzerland. This article is an open access article distributed under the terms and conditions of the Creative Commons Attribution (CC BY) license (<https://creativecommons.org/licenses/by/4.0/>).

1. Introduction

LLC topology has developed rapidly in recent decades. The applications are becoming increasingly extensive [1–5]. From the server power supply to the wireless charger to the electric vehicle charger, the applications are pervasive. The applied power level has increased from hundreds of watts to tens of kilowatts. Faced with increasing demand, LLC topology is still developing. For example, interleaved LLC improves the power level, but the problem of an unbalanced resonant current exists [6–8]. The three-phase LLC improves power level further while still maintaining the benefits, such as zero-voltage switching and high efficiency, and also improves disadvantages, such as a high output ripple current and unbalanced current. In addition, different transformer connection methods can lead to different circuit characteristics [9–11]. In general, the three-phase LLC has two types of transformer connections: one is Y-connection, and the other is Δ -connection. Y-connection such as Figure 1 is suitable for high-voltage applications, and Δ -connection is suitable for high-current places [12].

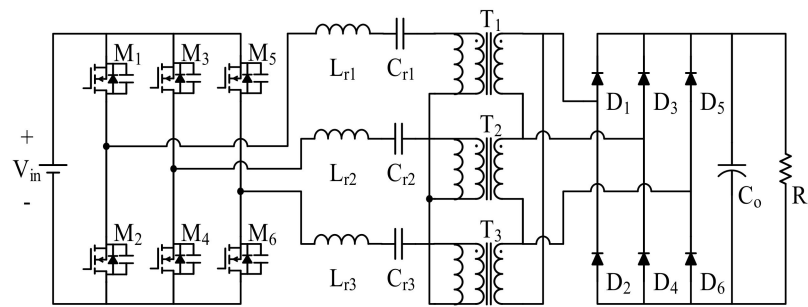


Figure 1. The conventional three-phase Y-Y connection LLC converter.

To increase the output power level further, this study proposes matrix transformer technology. Matrix transformers with different connection methods can disperse the stress of power components, improve heat dissipation problems, and increase the power level. When working with two transformers, there are four types of different connections that can improve different problems, such as series-series, series-parallel, parallel-parallel, and parallel-series connections [13–16]. Where [13] and [14] use two transformers to improve the power level, [15] uses a series-series connection to reduce the voltage stress of the transformers and ensure the currents are balanced on the primary side. The authors of [16] use a series-parallel connection to reduce the turns of the primary windings and current stress on the secondary windings. In addition, the conduction loss of rectifier diodes is also reduced. The authors of [17] use a parallel-series connection to achieve a very high step-up ratio (up to 650) as well as high voltage operation (~ 2 -kV). In [18,19], the authors use parallel-series connections to improve performance by reducing the turns of primary windings, decreasing the loss of coils, and reducing cross-regulation problems. In addition to the above voltage/current stress and power level effects, the matrix transformer can be used in planar transformers to improve circuit performance. In papers [20,21], matrix transformers were used to increase the possibilities of the circuit. With integrated transformer technology and advances in high-frequency technology, these two studies not only achieve a high step-down voltage and high efficiency, but also promote switching frequency to 1-MHz. Moreover, the matrix transformer method can be applied to many topologies, for example, the LLC converter [22], AC-DC inverter [23] and flyback converter [24]. The height of double transformers can also be reduced to facilitate occasions with height restrictions. In brief, a series/parallel connection can reduce the voltage/current stress of transformers, and more importantly, matrix transformers can increase the possibilities of the circuit. This study combines double-transformer technology and three-phase Y-Y LLC topology to verify and realize the above advantages.

For the analysis of the three-phase LLC resonant converter with matrix transformers, this paper will first introduce the composition of the proposed converter, then use a frequency-domain analysis to derive the curve of the voltage transfer ratio of the proposed converter. Next, it will introduce the operation principle, a time-domain analysis of different operating states, and a control block diagram. In Section 3, it will provide the components selection and a loss analysis. Finally, the experimental results of the three-phase LLC resonant converter with matrix transformers prototype will be presented. The input voltage is 800-VDC, the output voltage is 100-VDC, and the max output power is 20-kW. The highest efficiency is 97.61%.

2. Three-Phase LLC Resonant Converter with Matrix Transformers

Figure 2 shows the schematic of the three-phase LLC resonant converter with matrix transformers. The topology is composed of three sets of half-bridge LLC. Each half bridge consists of a series resonant tank and a separate set of transformers (T_{1A} and T_{1B}). Three sets of transformers are connected to one another in a Y-type structure at the primary side. Therefore, the voltage stress on the primary side of the transformer is reduced, given the series voltage division, and the current stress on the secondary side is halved because of

the parallel connection. Given the reduction of voltage and current stress, transformers and rectifier diodes will have more flexible choices. The heat dissipation capacity is also good.

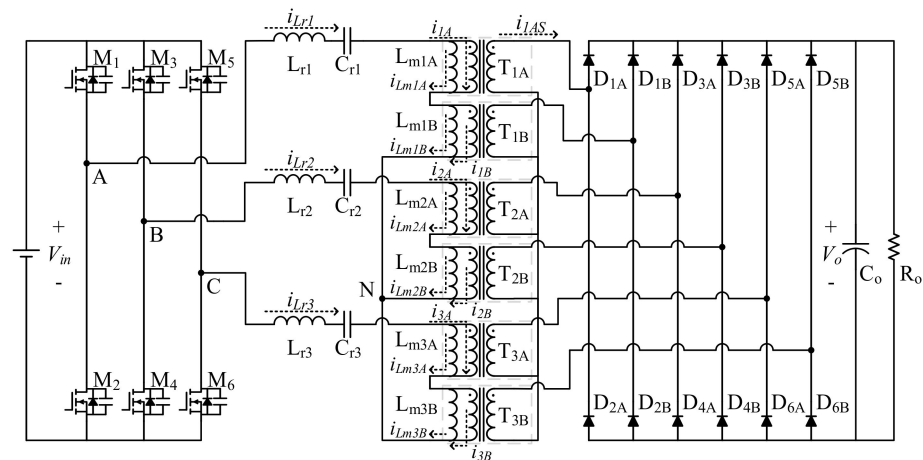


Figure 2. Schematic of the proposed three-phase LLC resonant converter with matrix transformers.

The common point N of Y-connected matrix transformers should be floating. The turns ratio of all transformers is $n:1$. Transformers TA and TB can be freely selected to be connected in parallel or to output individually. The control method is pulse frequency modulation. Each set of half-bridge signals is in 120° phase shift, and each duty cycle is almost 50%.

This section will provide an analysis of the voltage transfer ratio by using a first harmonic analysis (FHA) of the proposed converter and will introduce circuit operation in different states (regions 1 and 2) and a time-domain analysis. Where Region 1 is the region in which the switching frequency is higher than the first frequency fr_1 , Region 2 is the region in which the switching frequency is lower than the first frequency fr_1 . Circuit analysis is complicated, and thus simplifying the analysis is necessary. The following are our assumptions:

1. The parasitic capacitance of the MOSFET is neglected.
2. Output capacitance C_o is large enough so that the output voltage is a constant value.
3. All components are ideal such that the conduction losses of all switches and diodes are neglected.

2.1. Calculation of Voltage Transfer Ratio Curve by FHA

This study uses the FHA method to derive the curve of the voltage transfer ratio. The transfer ratio ($G = \frac{nV_o}{V_{in}}$) can be derived by calculating the relationship between the voltage and the current in the first harmonic type and the one cycle. Figure 3 is the single-phase schematic of the proposed converter. The transfer ratio G can be redefined as (1).

$$G = \frac{V_o}{V_{in}} = \frac{V_o}{I_o} \cdot \frac{I_o}{I_A} \cdot \frac{I_A}{V_{aN}} \cdot \frac{V_{aN}}{V_{AN}} \cdot \frac{V_{AN}}{V_{in}} \quad (1)$$

The separate calculation results of (1) are listed in Table 1. All results are presented with the FHA coefficient.

Table 1. Design parameters of the experiment and simulation.

Separate Part	Calculation Results
$\frac{V_o}{I_o}$	R_o
$\frac{I_o}{I_A}$	$\frac{6n}{\pi}$
$\frac{I_A}{V_{aN}}$	$\frac{\pi^2}{24n^2 R_o}$
$\frac{V_{aN}}{V_{AN}}$	$ H(j\omega) $
$\frac{V_{AN}}{V_{in}}$	$\frac{2}{\pi}$

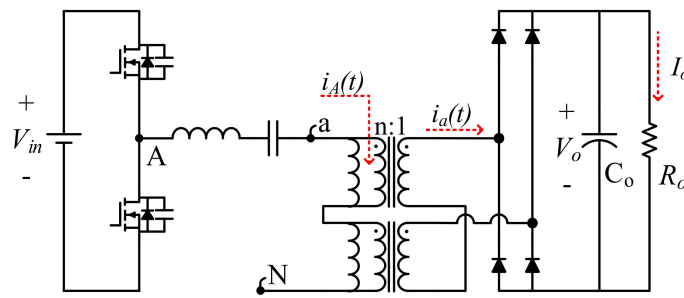


Figure 3. Single-phase schematic of the proposed converter.

All calculation results are multiplied to obtain the voltage transfer ratio G .

$$G = \frac{|H(j\omega)|}{2n} \quad (2)$$

The frequency response $|H(j\omega)|$ can be depicted as Figures 4 and 5. The definitions of all signs are as follows:

$$\text{Frequency response } |H(j\omega)| = \frac{1}{\sqrt{\left[\left(\frac{\omega_1^2}{\omega_2^2} - \frac{\omega_1^2}{\omega^2}\right)\frac{1}{K}\right]^2 + \left[Q\left(\frac{\omega}{\omega_1} - \frac{\omega_1}{\omega}\right)\right]^2}}$$

Switching angular frequency $\omega = 2\pi f$

First resonant angular frequency $\omega_1 = 2\pi f r_1$

Second resonant angular frequency $\omega_2 = 2\pi f r_2$

Quality factor value $Q = \frac{\sqrt{L_r/C_r}}{n^2 R_o}$

Ratio of magnetizing inductance to resonant inductance $K = \frac{L_m}{L_r}$

f is switching frequency

First resonant frequency $f r_1 = \frac{1}{2\pi\sqrt{L_r C_r}}$

Second resonant frequency $f r_2 = \frac{1}{2\pi\sqrt{(L_r + L_m) C_r}}$

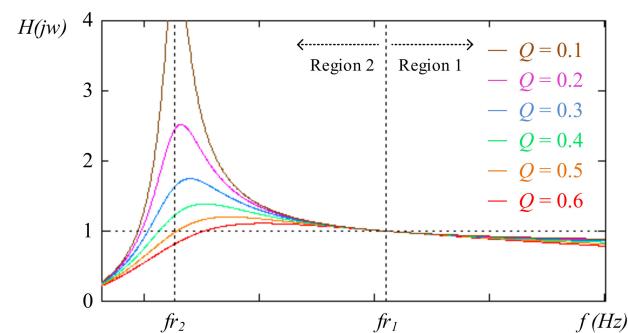


Figure 4. Relationship between transfer ratio and Q value.

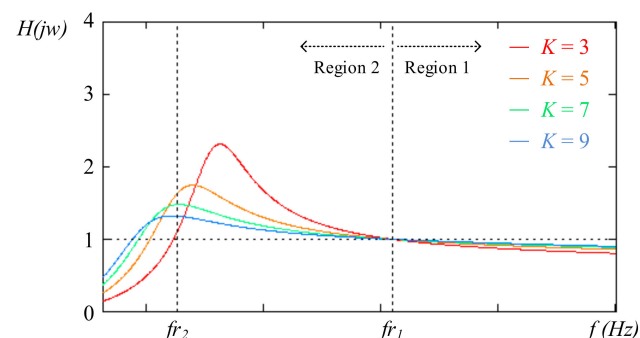


Figure 5. Relationship between transfer ratio and K value.

The condition of Figure 4 is the transfer ratio curve of different Q values under the condition of fixed $K = 5$, and the condition of Figure 5 is the transfer ratio curve of different K values under the condition of fixed $Q = 0.3$.

Figures 4 and 5 show that the operate condition depends on the switching frequency and slope of the transfer ratio curve. If the circuit operates at the positive slope, it will be inductive; otherwise, it will be capacitive. If the switching frequency operates at higher than fr_1 (Region 1), the magnetizing inductor will be clamped in all conditions and will not participate in resonance. If the switching frequency operates lower than the fr_2 (Region 2) and positive slope, the magnetizing inductor will decouple in specific stages and participate in resonance. The next section will introduce the operation principle of the two regions.

2.2. Operation Principle and Time Domain Analysis of the Three-Phase LLC Resonant Converter with Matrix Transformers

The operation waveforms of the three-phase LLC resonant converter with matrix transformers in Region 1 are shown in Figure 6. Among them, $v_{gsM1} \sim v_{gsM6}$ are control signals of six MOSFETs $M_1 \sim M_6$. i_{Lr1} , i_{Lr2} , and i_{Lr3} are the resonant inductor current. i_{Lm1A} , i_{Lm2A} , and i_{Lm3A} are the magnetizing inductor current. i_{1A} , i_{2A} , and i_{3A} are the transformer secondary current. i_{D1A} , i_{D2A} , i_{D1B} , and i_{D2B} are the rectifier diodes current. The above waveforms definitions can be found in Figure 2. The operation stage in a cycle can be divided into 12 parts ($t_0 \sim t_{12}$). Given that the positive and negative cycles are symmetrical, only the positive cycle will be explained.

Moreover, for the mathematical expression of the resonant tank, the following definitions are required:

$$Z_o = \sqrt{\frac{L_r}{C_r}}, Z_o \text{ is the characteristic impedance.}$$

The statement diagram of each stage is shown in Figure 6.

Stage 1 ($t_0 \sim t_1$):

As shown in Figure 7a, switches M4 and M5 are turned on and switches M2, M3, and M6 are turned off. Given the continuity of the resonant current i_{Lr1} , the body diode of switch M1 is turned on. Voltage v_{AN} changes to $\frac{1}{3}V_{in}$ from $-\frac{1}{3}V_{in}$ and v_{aN} is $-\frac{2}{3}nV_o$. The current value i_{1A} drops quickly to 0, and then this stage ends. In Region 1, all transformers transfer energy to the secondary side. The resonant inductor current i_{Lr1} , the resonant capacitor voltage v_{Cr1} , and the magnetizing inductor current i_{Lm1A} are shown as follows:

$$i_{Lr1}(t) = i_{Lr}(t_0) \cdot \cos[\omega(t - t_0)] + \frac{\frac{1}{3}V_{in} + \frac{2}{3}nV_o - v_{Cr}(t_0)}{Z_o} \sin[\omega(t - t_0)] \quad (3)$$

$$v_{Cr1}(t) = Z_o \cdot i_{Lr}(t_0) \sin[\omega(t - t_0)] - \left[\frac{1}{3}V_{in} + \frac{2}{3}nV_o - v_{Cr}(t_0) \right] \cos[\omega(t - t_0)] + \frac{1}{3}V_{in} + \frac{2}{3}nV_o \quad (4)$$

$$i_{Lm1A}(t) = i_{Lm1A}(t_0) - \frac{1}{3} \frac{nV_o}{L_{m1A}}(t - t_0) \quad (5)$$

Stage 2 ($t_1 \sim t_2$):

In this stage, switches M4 and M5 keep turning on, and switches M2, M3, and M6 keep turning off. Switch M1 will turn on after dead time. The current i_{1A} drops to 0 and turns to the positive current of Stage 1. Voltage v_{aN} changes to $\frac{2}{3}nV_o$. The resonant inductor current i_{Lr1} , the resonant capacitor voltage v_{Cr1} , and the magnetizing inductor current i_{Lm1A} are shown as follows:

$$i_{Lr1}(t) = i_{Lr}(t_1) \cdot \cos[\omega(t - t_1)] + \frac{\frac{1}{3}V_{in} - \frac{2}{3}nV_o - v_{Cr}(t_1)}{Z_o} \sin[\omega(t - t_1)] \quad (6)$$

$$v_{Cr1}(t) = Z_o \cdot i_{Lr}(t_1) \sin[\omega(t - t_1)] - \left[\frac{1}{3}V_{in} - \frac{2}{3}nV_o - v_{Cr}(t_1) \right] \cos[\omega(t - t_1)] + \frac{1}{3}V_{in} - \frac{2}{3}nV_o \quad (7)$$

$$i_{Lm1A}(t) = i_{Lm1A}(t_1) + \frac{1}{3} \frac{nV_o}{L_{m1A}}(t - t_1) \quad (8)$$

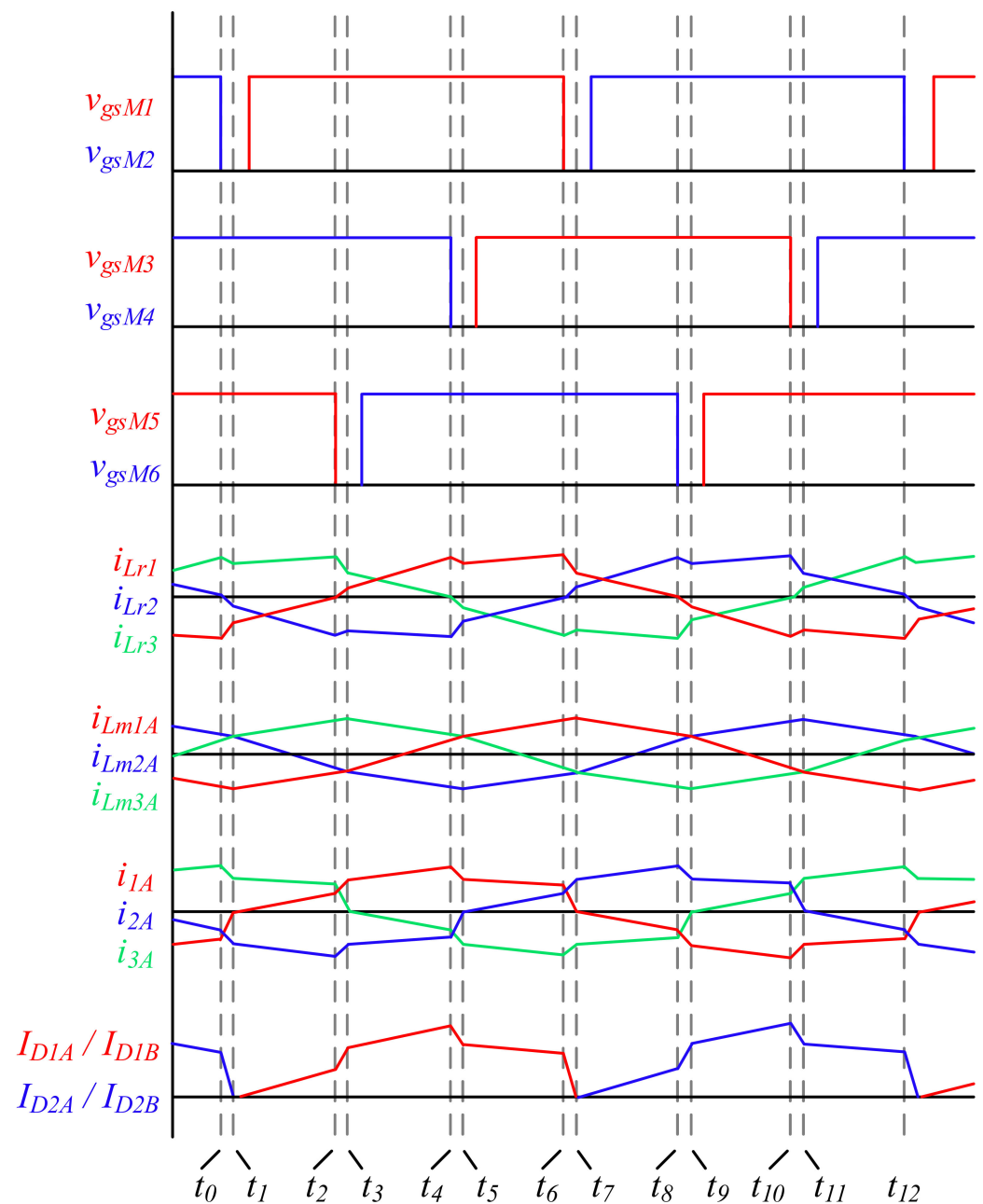


Figure 6. Operation waveforms of the three-phase LLC resonant converter with matrix transformers in Region 1.

Stage 3 (t_2 – t_3):

As shown in Figure 7c, switches M_1 and M_4 are turned on, and switches M_2 , M_3 , and M_5 are turned off. Given the continuity of the resonant current i_{Lr3} , the body diode of switch M_6 is turned on. Voltage v_{aN} changes to $\frac{2}{3}V_{in}$ from $\frac{1}{3}V_{in}$, and V_{aN} keeps $\frac{2}{3}nV_o$. The current value i_{3A} drops quickly to 0, and this stage ends. The resonant inductor current i_{Lr1} , the resonant capacitor voltage v_{Cr1} , and the magnetizing inductor current i_{Lm1A} are shown as follows:

$$i_{Lr1}(t) = i_{Lr}(t_2) \cdot \cos[\omega(t - t_2)] + \frac{\frac{2}{3}V_{in} - \frac{2}{3}nV_o - v_{Cr}(t_2)}{Z_o} \sin[\omega(t - t_2)] \quad (9)$$

$$v_{Cr1}(t) = Z_o \cdot i_{Lr}(t_2) \sin[\omega(t - t_2)] - \left[\frac{2}{3}V_{in} - \frac{2}{3}nV_o - v_{Cr}(t_2) \right] \cos[\omega(t - t_2)] + \frac{2}{3}V_{in} - \frac{2}{3}nV_o \quad (10)$$

$$i_{Lm1A}(t) = i_{Lm1A}(t_2) + \frac{1}{3} \frac{nV_o}{L_{m1A}} (t - t_2) \quad (11)$$

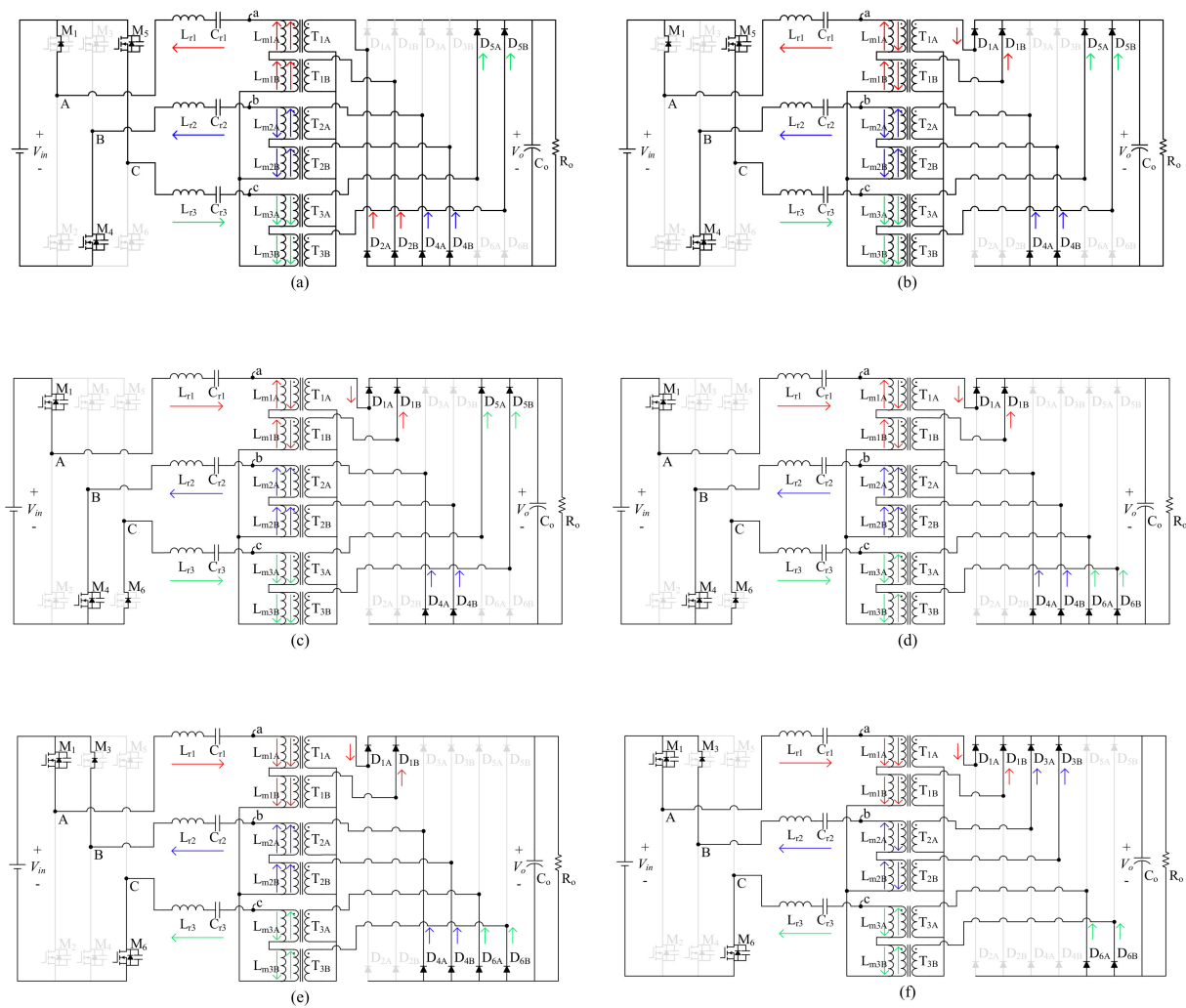


Figure 7. Operation station of the three-phase LLC resonant converter with matrix transformers in Region 1 at (a) Stage 1, (b) Stage 2, (c) Stage 3, (d) Stage 4, (e) Stage 5, and (f) Stage 6.

Stage 4 (t_3 – t_4):

In Stage 4, switches M_1 and M_4 keep turning on, and switches M_2 , M_3 , and M_5 keep turning off. Switch M_1 turns on after dead time. The current value i_{3A} drops to 0 at Stage 3 and turns to negative current at this stage. Voltage v_{aN} changes to $\frac{4}{3}nV_o$. The resonant inductor current i_{Lr1} , the resonant capacitor voltage v_{Cr1} , and the magnetizing inductor current i_{Lm1A} are as follows:

$$i_{Lr1}(t) = i_{Lr}(t_3) \cdot \cos[\omega(t - t_3)] + \frac{\frac{2}{3}V_{in} - \frac{4}{3}nV_o - v_{Cr}(t_3)}{Z_o} \sin[\omega(t - t_3)] \quad (12)$$

$$v_{Cr1}(t) = Z_o \cdot i_{Lr}(t_3) \sin[\omega(t - t_3)] - \left[\frac{2}{3}V_{in} - \frac{4}{3}nV_o - v_{Cr}(t_3) \right] \cos[\omega(t - t_3)] + \frac{2}{3}V_{in} - \frac{4}{3}nV_o \quad (13)$$

$$i_{Lm1A}(t) = i_{Lm1A}(t_3) + \frac{2}{3} \frac{nV_o}{L_{m1A}} (t - t_3) \quad (14)$$

Stage 5 (t_4 – t_5):

Following the same rule as in Stages 1 and 3, switches M_1 and M_6 are turned on, and switches M_2 , M_4 , and M_5 are turned off. Given the continuity of the resonant current i_{Lr2} , the body diode of switch M_3 is turned on. Voltage v_{aN} changes to $\frac{1}{3}V_{in}$ from $\frac{2}{3}V_{in}$, and voltage v_{aN} keeps $\frac{4}{3}nV_o$. The current value i_{2A} drops quickly to 0, and this stage ends. The resonant inductor current i_{Lr1} , the resonant capacitor voltage v_{Cr1} , and the magnetizing inductor current i_{Lm1A} are as follows:

$$i_{Lr1}(t) = i_{Lr}(t_4) \cdot \cos[\omega(t - t_4)] + \frac{\frac{1}{3}V_{in} - \frac{4}{3}nV_o - v_{Cr}(t_4)}{Z_o} \sin[\omega(t - t_4)] \quad (15)$$

$$v_{Cr1}(t) = Z_o \cdot i_{Lr}(t_4) \sin[\omega(t - t_4)] - \left[\frac{1}{3} V_{in} - \frac{4}{3} n V_o - v_{Cr}(t_4) \right] \cos[\omega(t - t_4)] + \frac{1}{3} V_{in} - \frac{4}{3} n V_o \quad (16)$$

$$i_{Lm1A}(t) = i_{Lm1A}(t_4) + \frac{2}{3} \frac{n V_o}{L_{m1A}} (t - t_4) \quad (17)$$

Stage 6 (t_5 – t_6):

In Stage 6, switches M_1 and M_6 keep turning on, and switches M_2 , M_4 , and M_5 keep turning off. Switch M_3 turns on after dead time. The current value i_{2A} drops to 0 at Stage 5 and turns to positive current at this stage. Voltage v_{aN} changes to $\frac{2}{3} n V_o$. The resonant inductor current i_{Lr1} , the resonant capacitor voltage v_{Cr1} , and the magnetizing inductor current i_{Lm1A} are as follows:

$$i_{Lr1}(t) = i_{Lr}(t_5) \cdot \cos[\omega(t - t_5)] + \frac{\frac{1}{3} V_{in} - \frac{2}{3} n V_o - v_{Cr}(t_5)}{Z_o} \sin[\omega(t - t_5)] \quad (18)$$

$$v_{Cr1}(t) = Z_o \cdot i_{Lr}(t_5) \sin[\omega(t - t_5)] - \left[\frac{1}{3} V_{in} - \frac{2}{3} n V_o - v_{Cr}(t_5) \right] \cos[\omega(t - t_5)] + \frac{1}{3} V_{in} - \frac{2}{3} n V_o \quad (19)$$

$$i_{Lm1A}(t) = i_{Lm1A}(t_5) + \frac{1}{3} \frac{n V_o}{L_{m1A}} (t - t_5) \quad (20)$$

Figure 8 shows the operation waveforms of the three-phase LLC resonant converter with matrix transformers in Region 2. The definition of all symbols is the same as Region 1. v_x is also the transformer primary voltage similar to v_{Lm} . The difference is that when the stage is 1, 3, and 5, voltage v_{Lm} is related to output voltage. When the stage is 2, 4, and 6, the transformer is decoupled. Thus, voltage v_{Lm} is a variable value.

Stage 1 (t_0 – t_1):

As shown in Figure 9a, switches M_4 and M_5 are turned on, and switches M_2 , M_3 , and M_6 are turned off. Given the continuity of the resonant current i_{Lr1} , the body diode of switch M_1 is turned on. Voltage v_{AN} changes to $\frac{1}{3} V_{in}$ from $-\frac{1}{3} V_{in}$, and voltage V_{aN} is $-\frac{2}{3} n V_o$. The current value i_{1A} rises from 0, and the current value i_{1B} drops to 0; then, this stage ends. In this stage, all transformers transfer energy to the secondary side. The resonant inductor current i_{Lr1} , the resonant capacitor voltage v_{Cr1} , and the magnetizing inductor current i_{Lm1A} are as follows:

$$i_{Lr1}(t) = i_{Lr}(t_0) \cdot \cos[\omega(t - t_0)] + \frac{\frac{1}{3} V_{in} + \frac{2}{3} n V_o - v_{Cr}(t_0)}{Z_o} \sin[\omega(t - t_0)] \quad (21)$$

$$v_{Cr1}(t) = Z_o i_{Lr}(t_0) \sin[\omega(t - t_0)] - \left[\frac{1}{3} V_{in} + \frac{2}{3} n V_o - v_{Cr}(t_0) \right] \cos[\omega(t - t_0)] + \left(\frac{1}{3} V_{in} + \frac{2}{3} n V_o \right) \quad (22)$$

$$i_{Lm1A}(t) = i_{Lm1A}(t_0) - \frac{1}{3} \frac{n V_o}{L_{m1A}} (t - t_0) \quad (23)$$

Stage 2 (t_1 – t_2):

In this stage, switches M_1 , M_4 , and M_5 keep turning on, and switches M_2 , M_3 , and M_6 keep turning off. The current value i_{3A} keeps 0; thus, transformers T_{3A} and T_{3B} are decoupling. Given the decoupling, the transformer voltage depends on the divided impedance between all resonance tanks and the output load. Voltage v_{aN} is defined as $v_x(t)$. The resonant inductor current i_{Lr1} , the resonant capacitor voltage v_{Cr1} , and magnetizing inductor current i_{Lm1A} are as follows:

$$i_{Lr1}(t) = i_{Lr}(t_1) \cdot \cos[\omega(t - t_1)] + \frac{\frac{1}{3} V_{in} - v_x(t) - v_{Cr}(t_1)}{Z_o} \sin[\omega(t - t_1)] \quad (24)$$

$$v_{Cr1}(t) = Z_o i_{Lr}(t_1) \sin[\omega(t - t_1)] - \left[\frac{1}{3} V_{in} - v_x(t) - v_{Cr}(t_1) \right] \cos[\omega(t - t_1)] + \left(\frac{1}{3} V_{in} - v_x(t) \right) \quad (25)$$

$$i_{Lm1A}(t) = i_{Lm1A}(t_1) + \frac{1}{2} \frac{v_x(t)}{L_{m1A}} (t - t_1) \quad (26)$$

Stage 3 (t_2 – t_3):

As shown in Figure 9c, switches M_1 and M_4 are turned on, and switches M_2 , M_3 , and M_5 are turned off. Given the continuity of the resonant current i_{Lr3} , the body diode of switch M_6 is turned on. Voltage v_{AN} changes to $\frac{2}{3} V_{in}$ from $\frac{1}{3} V_{in}$, and voltage v_{aN} changes to $\frac{4}{3} n V_o$ from v_x . The current value i_{3A} rises from 0, and the current value i_{2A} drops to 0; then, this stage ends. In this stage, all

transformers transfer energy to the secondary side. The resonant inductor current i_{Lr1} , the resonant capacitor voltage v_{Cr1} , and the magnetizing inductor current i_{Lm1A} are as follows:

$$i_{Lr1}(t) = i_{Lr}(t_2) \cdot \cos[\omega(t - t_2)] + \frac{\frac{2}{3}V_{in} - \frac{4}{3}nV_o - v_{Cr}(t_2)}{Z_o} \sin[\omega(t - t_2)] \quad (27)$$

$$v_{Cr1}(t) = Z_o \cdot i_{Lr}(t_2) \sin[\omega(t - t_2)] - \left[\frac{2}{3}V_{in} - \frac{4}{3}nV_o - v_{Cr}(t_2) \right] \cos[\omega(t - t_2)] + \left(\frac{2}{3}V_{in} - \frac{4}{3}nV_o \right) \quad (28)$$

$$i_{Lm1A}(t) = i_{Lm1A}(t_2) + \frac{2}{3} \frac{nV_o}{L_{m1A}}(t - t_2) \quad (29)$$

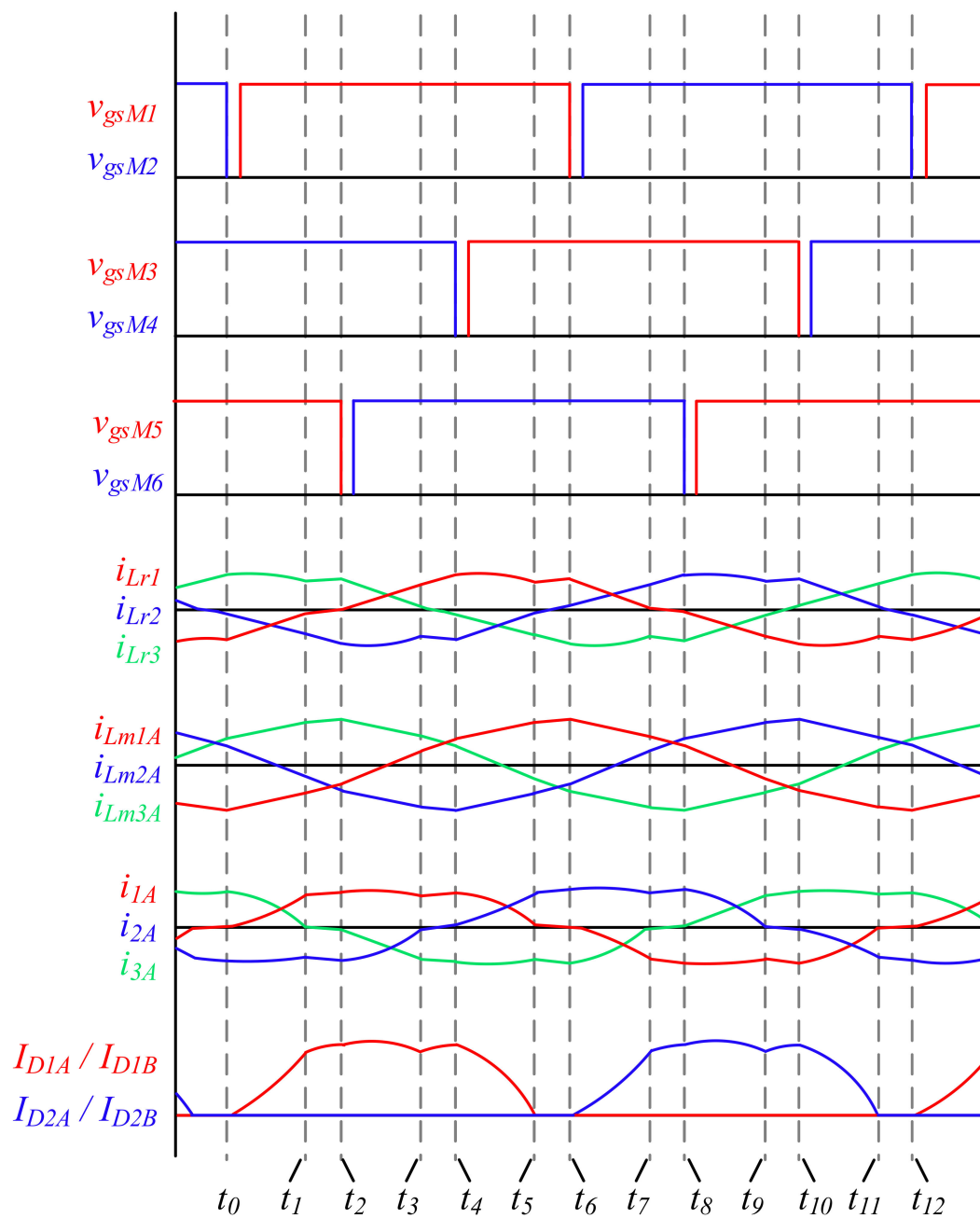


Figure 8. Operation waveforms of the three-phase LLC resonant converter with matrix transformers in Region 2.

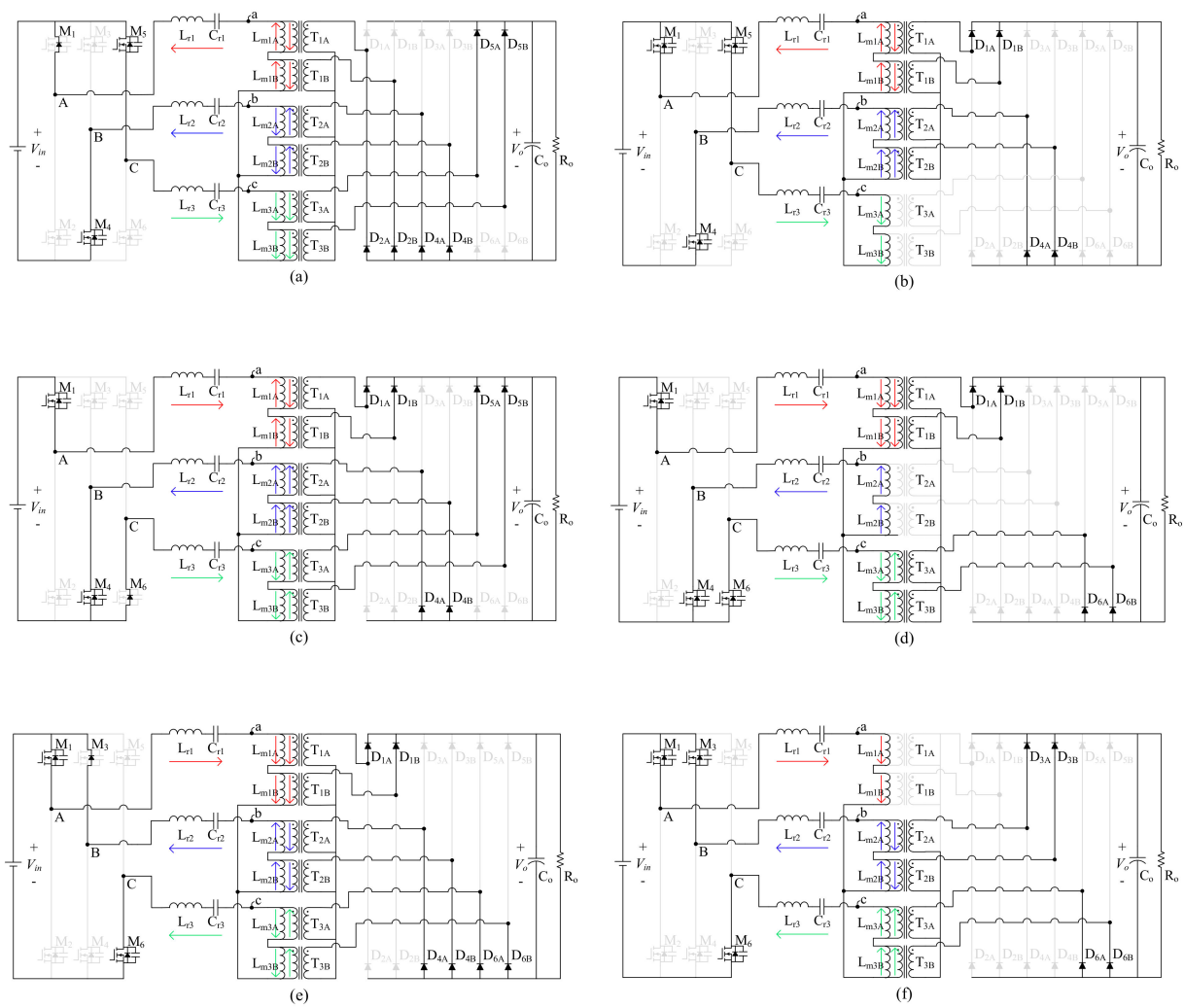


Figure 9. Operation station of the three-phase LLC resonant converter with matrix transformers in Region 2 at (a) Stage 1, (b) Stage 2, (c) Stage 3, (d) Stage 4, (e) Stage 5, and (f) Stage 6.

Stage 4 (t_3 – t_4):

In this stage, switches M_1 , M_4 , and M_6 keep turning on, and switches M_2 , M_3 , and M_5 keep turning off. The current value i_{2A} keeps 0; thus, transformer T_{2A} and T_{2B} are decoupling. Given the decoupling, the transformer voltage depends on the divided impedance between all resonance tanks and the output load. Voltage v_{aN} is defined as $v_x(t)$. The resonant inductor current i_{Lr1} , the resonant capacitor voltage v_{Cr1} , and the magnetizing inductor current i_{Lm1A} are as follows:

$$i_{Lr1}(t) = i_{Lr}(t_3) \cdot \cos[\omega(t - t_3)] + \frac{2}{3} \frac{V_{in} - v_x(t) - v_{Cr}(t_3)}{Z_o} \sin[\omega(t - t_3)] \quad (30)$$

$$v_{Cr1}(t) = Z_o \cdot i_{Lr}(t_3) \sin[\omega(t - t_3)] - \left[\frac{2}{3} V_{in} - v_x(t) - v_{Cr}(t_3) \right] \cos[\omega(t - t_3)] + \left(\frac{2}{3} V_{in} - v_x(t) \right) \quad (31)$$

$$i_{Lm1A}(t) = i_{Lm1A}(t_3) + \frac{1}{2} \frac{v_x(t)}{L_{m1A}} (t - t_3) \quad (32)$$

Stage 5 (t_4 – t_5):

As shown in Figure 9e, switches M_1 and M_6 are turned on, and switches M_2 , M_4 , and M_5 are turned off. Given the continuity of the resonant current i_{Lr2} , the body diode of switch M_3 is turned on. Voltage v_{aN} changes to $\frac{1}{3} V_{in}$ from $\frac{2}{3} V_{in}$, and voltage v_{aN} changes to $\frac{2}{3} n V_o$ from v_x . The current value i_{2A} rises from 0, and the current value i_{1A} drops to 0; then, this stage ends. In this stage, all

transformers transfer energy to the secondary side. The resonant inductor current i_{Lr1} , the resonant capacitor voltage v_{Cr1} , and the magnetizing inductor current i_{Lm1A} are as follows:

$$i_{Lr1}(t) = i_{Lr}(t_4) \cdot \cos[\omega(t - t_4)] + \frac{\frac{1}{3}V_{in} - \frac{2}{3}nV_o - v_{Cr}(t_4)}{Z_o} \sin[\omega(t - t_4)] \quad (33)$$

$$v_{Cr1}(t) = Z_o i_{Lr}(t_4) \sin[\omega(t - t_4)] - \left[\frac{1}{3}V_{in} - \frac{2}{3}nV_o - v_{Cr}(t_4) \right] \cos[\omega(t - t_4)] + \left(\frac{1}{3}V_{in} - \frac{2}{3}nV_o \right) \quad (34)$$

$$i_{Lm1A}(t) = i_{Lm1A}(t_4) + \frac{1}{3} \frac{nV_o}{L_{m1A}} (t - t_4) \quad (35)$$

Stage 6 (t_5 – t_6):

In this stage, switches M_1 , M_3 , and M_6 keep turning on, and switches M_2 , M_4 , and M_5 keep turning off. The current value i_{1A} keeps 0; thus, transformers T_{1A} and T_{1B} are decoupling. Given the decoupling, the transformer voltage depends on the divided impedance between all resonance tanks and the output load. The voltage v_{aN} is defined as $v_x(t)$. The resonant inductor current i_{Lr1} , the resonant capacitor voltage v_{Cr1} , and the magnetizing inductor current i_{Lm1A} are shown as follows:

$$i_{Lr1}(t) = i_{Lr}(t_5) \cdot \cos[\omega(t - t_5)] + \frac{\frac{1}{3}V_{in} - v_x(t) - v_{Cr}(t_5)}{Z_o} \sin[\omega(t - t_5)] \quad (36)$$

$$v_{Cr1}(t) = Z_o i_{Lr}(t_5) \sin[\omega(t - t_5)] - \left[\frac{1}{3}V_{in} - v_x(t) - v_{Cr}(t_5) \right] \cos[\omega(t - t_5)] + \left(\frac{1}{3}V_{in} - v_x(t) \right) \quad (37)$$

$$i_{Lm1A}(t) = i_{Lm1A}(t_5) + \frac{1}{2} \frac{v_x(t)}{L_{m1A}} (t - t_5) \quad (38)$$

2.3. Control Block Diagram

A control block diagram of the three-phase LLC resonant converter with matrix transformers is shown in Figure 10. The control function includes an error amplifier of the PI controller and voltage control oscillator (VCO) for regulated output voltage, and uses the driver IC to isolate the primary and secondary sides.

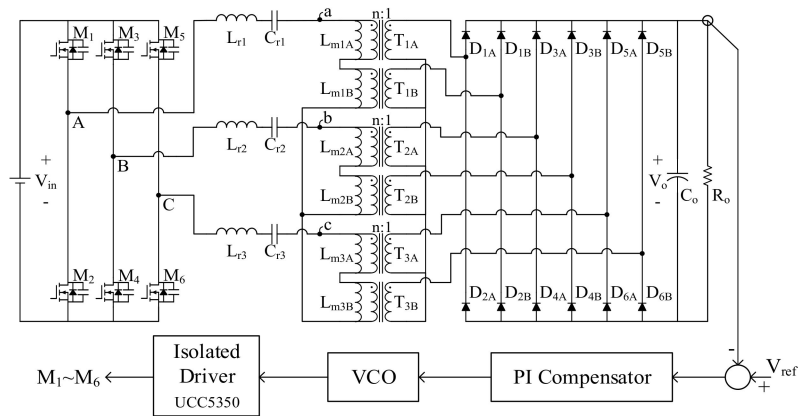


Figure 10. Control block diagram.

3. Components Selection and Loss Analysis

Before implementing the experimental circuit, a component selection and loss analysis are necessary. Table 2 is the prototype specification of the three-phase LLC resonant converter with matrix transformers. All component designs and selection are as follows:

Table 2. Prototype specification.

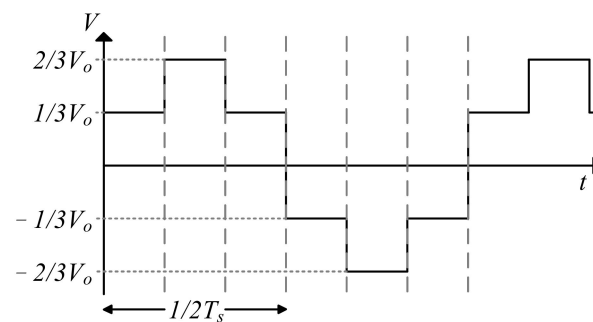
Item	Value
Input voltage V_{in}	800 V
Output voltage V_o	100 V
Output current I_o	200 A
Output power P_o	20 kW
Switching frequency	40~250 kHz

The results of the voltage transfer ratio show that the proposed converter and traditional LLC are the same. Therefore, the circuit design and component selection are also similar. Differences are the voltage waveform of the transformers and the utilization of matrix transformers to replace the single transformer. The matrix transformers are series at the primary side and parallel at the secondary side. This kind of composition exists and gains 0.5 times in the circuit. Efficiency is better when operating at the resonance frequency. Thus, the transformer turns ratio can be calculated as follows:

$$n = \frac{V_{in}}{2 \cdot V_o} = \frac{800}{2 \cdot 100} = 4$$

Figure 11 is the voltage waveform of matrix transformers at the secondary side. Derived from Faraday's formula, the maximum magnetic flux density B_{max} can be expressed as Equation (39).

$$B_{max} = \frac{\left(\frac{1}{3}V_o + \frac{2}{3}V_o + \frac{1}{3}V_o\right)\frac{1}{6}T_s}{2A_eN_s} 10^4 (\text{Tesla}) = \frac{1}{9} \frac{V_o}{A_eN_s f} 10^4 (\text{Tesla}) \quad (39)$$

**Figure 11.** Voltage stress of matrix transformers at secondary side.

After arranging the Equation (39) and plugging the magnetic material data, the minimum secondary turns N_s are presented as follows:

$$N_s = \frac{100 \text{ V} \cdot 10^4}{9 \cdot 5.3 \text{ cm} \cdot 40 \text{ kHz} \cdot 0.32 \text{ T}} = 1.638 \quad (40)$$

According to the minimum turns required to be an integer, the number of turns at the secondary side is 2. Therefore, the number of turns at the primary side is 8.

Through simulation, stress analysis loss, analysis, and choice of voltage transfer ratio curve, the component selection results are shown in Table 3. Table 4 provides the voltage/current stress relation formula of the MOSFET and diode. The simulation value is shown in Table 5. The calculation method of loss analysis is shown in Table 6, and the loss ratio distribution diagram is shown in Figure 11. The power components loss analysis includes the MOSFET, diode, transformer, and inductor. The symbols used in the calculation method and material data are described in Table 7.

Figure 12 shows the power loss of the conventional three-phase Y-Y LLC and the three-phase Y-Y LLC with matrix transformers at 50% and 100% load, respectively. The estimation of component loss only includes the MOSFET, diode, transformer, and inductor. The converter with matrix transformer's total losses at 50% and 100% load are 220-W and 442-W. The estimated efficiency is 97.9% and 97.8%. Results show that the main power loss is the conduction loss of the rectifier diode. The power loss of each rectifier diode and transformer at 100% load is about 24.4-W and 9.1-W. Compare this to the general three-phase Y-Y LLC resonant converter: the power loss of each rectifier diode and

transformer at 100% load would be up to about 56.8-W and 22.9-W. This means the matrix transformer method improves efficiency and makes component selection easier.

Table 3. Components list.

Item	Value
MOSFET	FF23MR12W1M1_B11
Diode	DSS2x101-02A
Transformer turns ratio	4:1
Magnetizing inductor	50 μ H
Resonant inductor	20 μ H
Magnetic material	3C95

Table 4. Relation formula of MOSFET and diode stress.

Item	Relation Formula
MOSFET	Voltage stress Current I_{RMS}
Diode	Voltage stress Average current

Table 5. Voltage/current stress simulation result of MOSFET and diode.

Item	50% Load	100% Load
MOSFET	Voltage stress Current I_{RMS}	800 V 10.09 A
Diode	Voltage stress Average current	100 V 17.20 A

Table 6. Calculation method of loss analysis.

Component	Loss Type	Calculation Method
MOSFET	Conduction loss Switching loss	$I_{MOSFET_RMS}^2 \cdot R_{DS_ON}$ $E_{off} \cdot f$
Diode	Conduction loss	$V_f \cdot I_{Diode_AVG}$
Magnetizing inductor	Core loss Copper loss	$P_{cv} \cdot V_e$ $I_{Tr_pri_RMS}^2 \cdot R_{pri} + I_{Tr_sec_RMS}^2 \cdot R_{sec}$
Resonant inductor	Core loss Copper loss	$P_{cv} \cdot V_e$ $I_{Lr_RMS}^2 \cdot R_{Lr}$

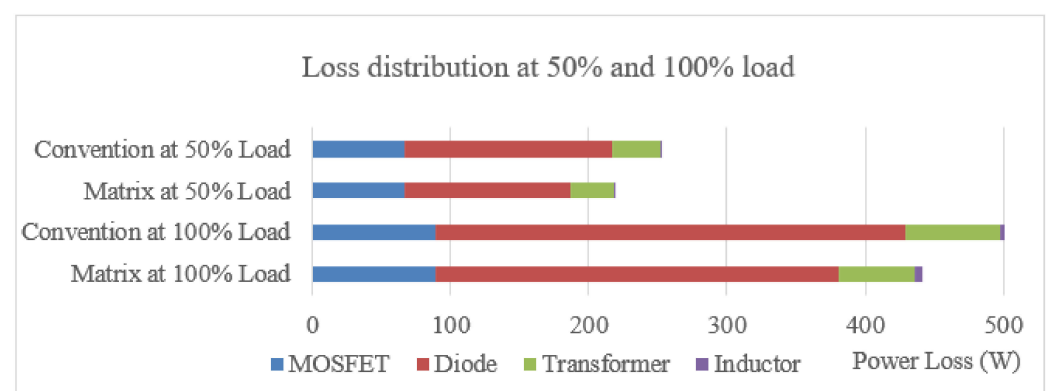


Figure 12. Loss ratio distribution at 50% and 100% load.

Table 7. Symbol description.

Item	Description
I_{MOSFET_RMS}	RMS current flow across the MOSFET
R_{DS_ON}	Resistance between the drain and source in MOSFET
E_{off}	Turn-off energy loss per pulse
P_{cv}	Core loss volume density
V_e	Effective core volume
A_e	Effective cross-sectional area
N_s	Number of turns
$I_{Tr_pri_RMS}$	RMS current flow across the transformer primary side
$I_{Tr_sec_RMS}$	RMS current flow across the transformer secondary side
I_{Lr_RMS}	RMS current flow across the resonant inductor
R_{pri}	Copper resistance of transformer primary side
R_{sec}	Copper resistance of transformer secondary side
R_{Lr}	Copper resistance of resonant inductor

4. Experimental Results

To verify the feasibility of dual-transformer technology, a 20-kW, input voltage 800-V and output voltage 100-V prototype is built and tested in this study. Figure 13 shows the MOSFET waveform of each low-side signal of the three-phase LLC resonant converter with matrix transformers.

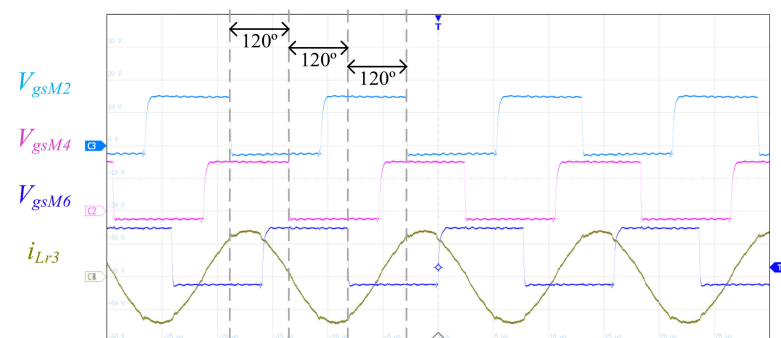


Figure 13. MOSFET waveform of the proposed converter (Time: 5 μ s/div; v_{gsM2} : 10 V/div; v_{gsM4} : 10 V/div; v_{gsM6} : 10 V/div; i_{Lr3} : 10 A/div).

In Figure 13, the phases of each MOSFET are 120° apart from each other. The following data show the waveform from 25% load to 100% load in Figures 14–17.

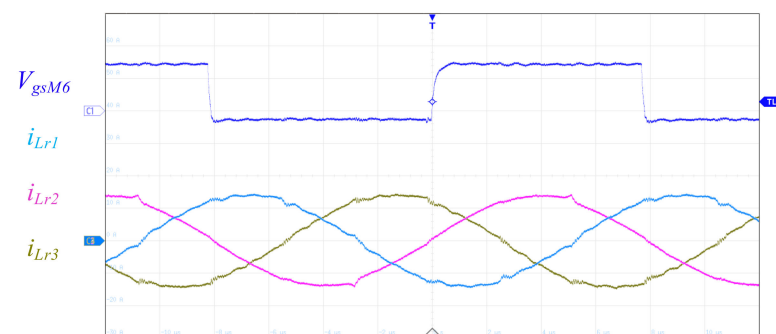


Figure 14. Operation waveform of the proposed converter at 25% load (Time: 2 μ s/div; v_{gsM6} : 10 V/div; i_{Lr1} : 10 A/div; i_{Lr2} : 10 A/div; i_{Lr3} : 10 A/div).

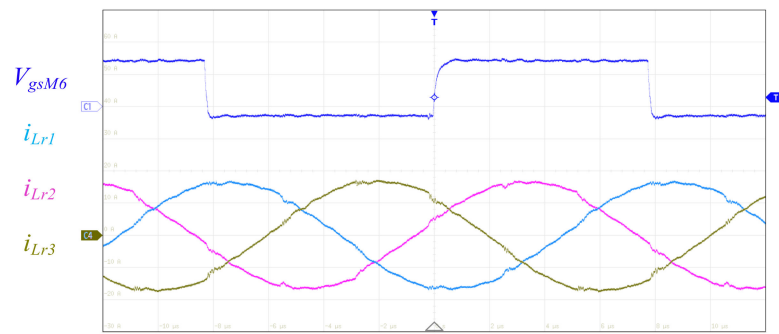


Figure 15. Operation waveform of the proposed converter at 50% load (Time: 2 μ s/div; v_{gsM6} : 10 V/div; i_{Lr1} : 10 A/div; i_{Lr2} : 10 A/div; i_{Lr3} : 10 A/div).

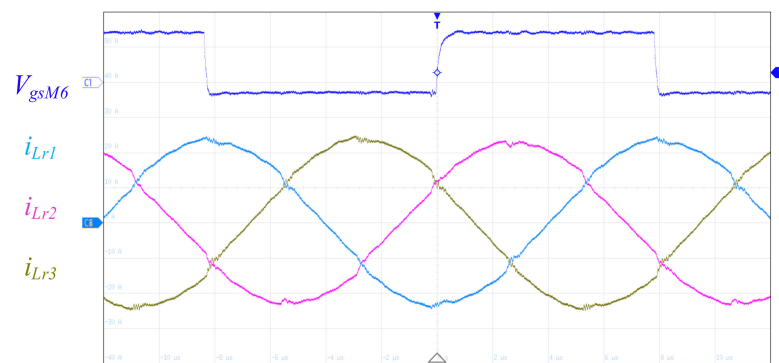


Figure 16. Operation waveform of the proposed converter at 75% load (Time: 2 μ s/div; v_{gsM6} : 10 V/div; i_{Lr1} : 10 A/div; i_{Lr2} : 10 A/div; i_{Lr3} : 10 A/div).

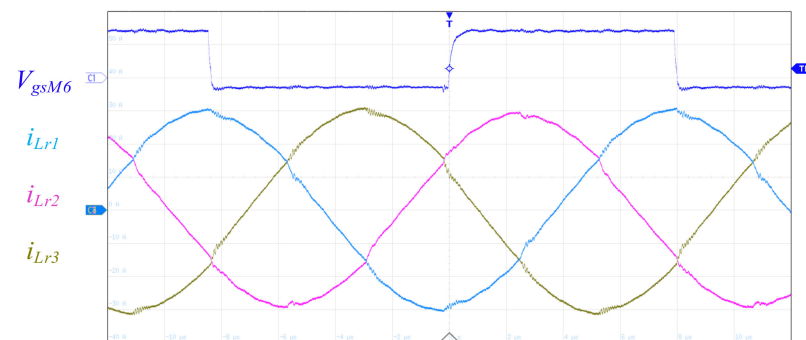


Figure 17. Operation waveform of the proposed converter at 100% load (Time: 2 μ s/div; v_{gsM6} : 10 V/div; i_{Lr1} : 10 A/div; i_{Lr2} : 10 A/div; i_{Lr3} : 10 A/div).

Figure 18 shows the zero voltage turn-on waveform at 25% load. The statement of MOSFET is zero-voltage switching. Figure 19 shows the wave form of the output voltage ripple at 100% load. The output voltage ripple is composed of two parts; one waveform is close to the switching frequency, whereas the other one is a higher frequency, which is caused by MOSFET switching noise. In Figure 19, the peak–peak value of the lower frequency voltage ripple v_o is approximately 1 V.

Given that the output transfer ratio is designed at the resonant point, the switching frequency almost does not change from light load to full load. The amplitudes of the three resonant currents are also closed, which means no unbalanced current problem occurs. Figure 20 shows the efficiency of the three-phase LLC resonant converter with matrix transformers. The highest efficiency is 97.61% at 110 A. Full load efficiency is 97.18%. Compared with the prior loss analysis, the experimental results are close to the loss analysis (96.2% at half load and 97.2% at full load). Figure 21 shows the prototype of the proposed converter, and Figure 22 shows the height of the proposed prototype.

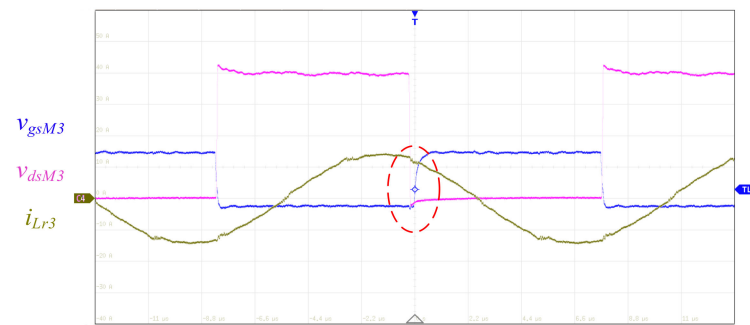


Figure 18. Operation waveform of zero-voltage turn on at 25% load (Time: 2.2 $\mu\text{s}/\text{div}$; v_{gsM3} : 10 V/div; v_{dsM3} : 200 V/div; i_{Lr3} : 10 A/div).

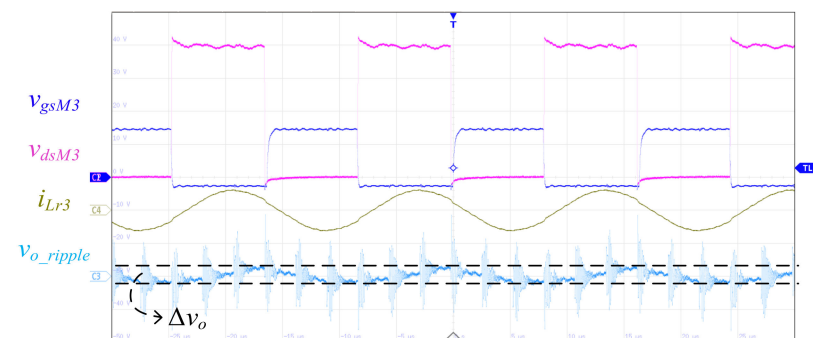


Figure 19. Operation waveform of output voltage ripple at 100% load (Time: 2.2 $\mu\text{s}/\text{div}$; v_{gsM3} : 10 V/div; v_{dsM3} : 200 V/div; i_{Lr3} : 50 A/div; v_{o_ripple} : 2 V/div).

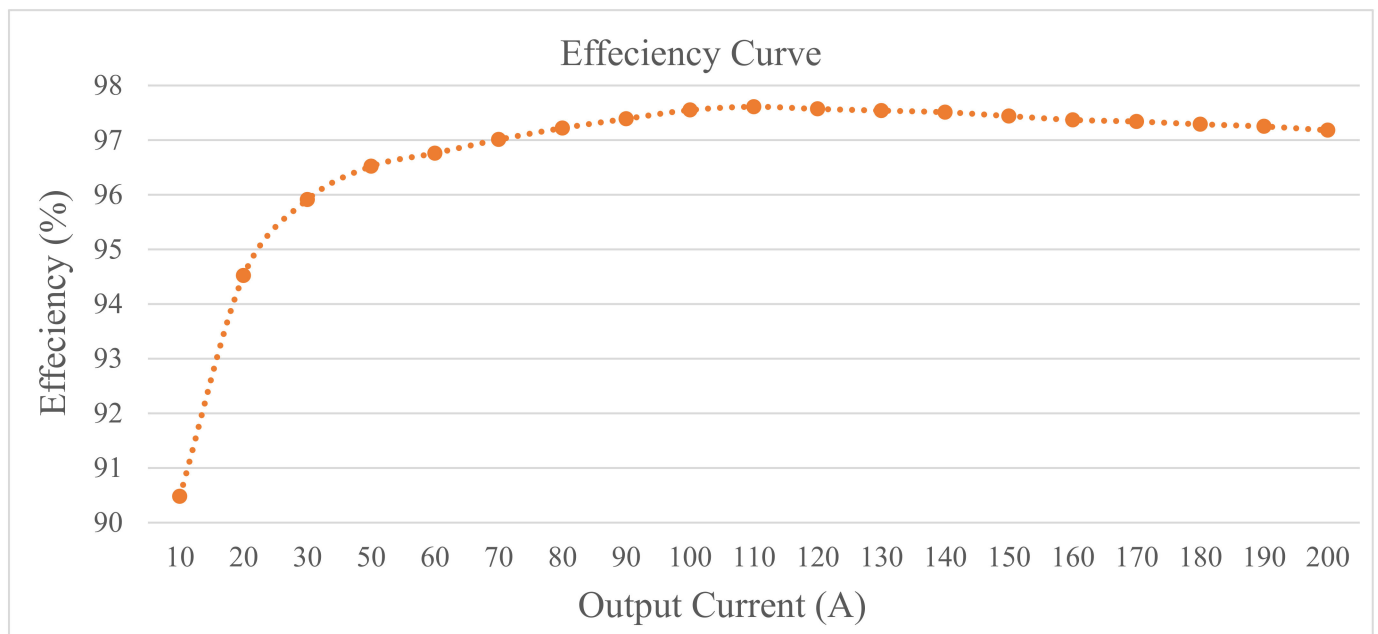


Figure 20. Efficiency of the three-phase LLC resonant converter with matrix transformers.

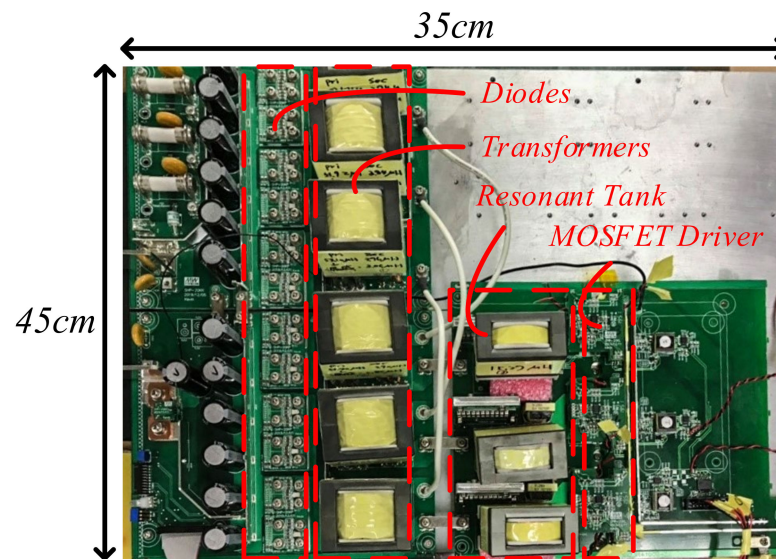


Figure 21. Prototype of the three-phase LLC resonant converter with matrix transformers.



Figure 22. Height of the three-phase LLC resonant converter with matrix transformers.

5. Conclusions

To increase the output power level of the three-phase LLC resonant converter with matrix transformers, this study proposes dual transformers to replace the original transformer and achieve this purpose. Circuit topology, operation mode, operation principle, time-domain analysis, and frequency analysis are all discussed in the article. It is proposed that this method can reduce transformer voltage/current stress and increase output power while maintaining the advantages of the original topology. Finally, a 20-kW prototype three-phase LLC resonant converter with matrix transformers is built, the experimental results verify the above analysis, and efficiency performance is high.

Author Contributions: Supervision, J.-Y.L.; Writing—Original Draft, Y.-F.L.; Writing—Review, P.-H.L. and H.-Y.Y.; Writing—Review & Editing, Y.-F.L. All authors have read and agreed to the published version of the manuscript.

Funding: This research received no external funding.

Institutional Review Board Statement: Not applicable.

Informed Consent Statement: Not applicable.

Data Availability Statement: Not applicable.

Conflicts of Interest: The authors declare no conflict of interest.

References

1. Zeng, J.; Zhang, G.; Yu, S.S.; Zhang, B.; Zhang, Y. LLC resonant converter topologies and industrial applications—A review. *Chin. J. Electr. Eng.* **2020**, *6*, 73–84. [\[CrossRef\]](#)
2. Musavi, F.; Craciun, M.; Gautam, D.S.; Eberle, W.; Dunford, W.G. An LLC resonant DC–DC converter for wide output voltage range battery charging applications. *IEEE Trans. Power Electron.* **2013**, *28*, 5437–5445. [\[CrossRef\]](#)
3. Duan, C.; Bai, H.; Guo, W.; Nie, Z. Design of a 2.5-kW 400/12-V high-efficiency DC/DC converter using a novel synchronous rectification control for electric vehicles. *IEEE Trans. Transp. Electr.* **2015**, *1*, 106–114. [\[CrossRef\]](#)
4. Sun, X.; Shen, Y.; Zhu, Y.; Guo, X. Interleaved boost-integrated LLC resonant converter with fixed-frequency PWM control for renewable energy generation applications. *IEEE Trans. Power Electron.* **2014**, *30*, 4312–4326. [\[CrossRef\]](#)
5. Zheng, C.; Chen, B.; Zhang, L.; Chen, R.; Lai, J.S. Design considerations of LLC resonant converter for contactless laptop charger. In *Proceedings of the 2015 IEEE Applied Power Electronics Conference and Exposition (APEC), Charlotte, NC, USA, 15–19 March 2015*; IEEE: New York, NY, USA, 2015; pp. 3341–3347.
6. Hu, Z.; Qiu, Y.; Wang, L.; Liu, Y.F. An interleaved LLC resonant converter operating at constant switching frequency. *IEEE Trans. Power Electron.* **2013**, *29*, 2931–2943. [\[CrossRef\]](#)
7. Xue, B.; Wang, H.; Liang, J.; Cao, Q.; Li, Z. Phase-shift modulated interleaved LLC converter with ultrawide output voltage range. *IEEE Trans. Power Electron.* **2020**, *36*, 493–503. [\[CrossRef\]](#)
8. Yu, K.; Du, J.; Ma, H. A novel current sharing method for multi-module LLC resonant converters. In *Proceedings of the IECON 2017-43rd Annual Conference of the IEEE Industrial Electronics Society, Beijing, China, 29 October–1 November 2017*; IEEE: New York, NY, USA, 2017; pp. 613–618.
9. Arshadi, S.A.; Ordóñez, M.; Eberle, W.; Craciun, M.; Botting, C. Three-phase LLC battery charger: Wide regulation and improved light-load operation. *IEEE Trans. Power Electron.* **2020**, *36*, 1519–1531. [\[CrossRef\]](#)
10. Rahman, A.N.; Lee, C.Y.; Chiu, H.J.; Hsieh, Y.C. Bidirectional three-phase LLC resonant converter. In *Proceedings of the 2018 IEEE Transportation Electrification Conference and Expo, Asia-Pacific (ITEC Asia-Pacific), Bangkok, Thailand, 6–9 June 2018*; IEEE: New York, NY, USA, 2018; pp. 1–5.
11. Fei, C.; Gadelrab, R.; Li, Q.; Lee, F.C. High-frequency three-phase interleaved LLC resonant converter with GaN devices and integrated planar magnetics. *IEEE J. Emerg. Sel. Top. Power Electron.* **2019**, *7*, 653–663. [\[CrossRef\]](#)
12. Jacobs, J.; Thommes, M.; De Doncker, R.W.A.A. A transformer comparison for three-phase single active bridges. In *Proceedings of the 2005 European Conference on Power Electronics and Applications, Dresden, Germany, 11–14 September 2005*; IEEE: New York, NY, USA, 2005; p. 10.
13. Lin, B.R.; Yang, W.R.; Chen, J.J.; Huang, C.L.; Yu, M.H. Interleaved LLC series converter with output voltage doubler. In *Proceedings of the 2010 International Power Electronics Conference-ECCE ASIA-, Sapporo, Japan, 21–24 June 2010*; IEEE: New York, NY, USA, 2010; pp. 92–98.
14. Lin, B.R.; Wu, S.F. Implementation of a series resonant converter with series–parallel transformers. *IET Power Electron.* **2011**, *4*, 919–926. [\[CrossRef\]](#)
15. Pittini, R.; Huang, L.; Zhang, Z.; Andersen, M.A. Primary parallel secondary series flyback converter (PPSSFC) with multiple transformers for very high step-up ratio in capacitive load charging applications. In *Proceedings of the 2014 IEEE Applied Power Electronics Conference and Exposition-APEC 2014, Fort Worth, TX, USA, 16–20 March 2014*; IEEE: New York, NY, USA, 2014; pp. 1440–1447.
16. Kim, H.S.; Jung, J.H.; Baek, J.W.; Kim, H.J. Analysis and design of a multioutput converter using asymmetrical PWM half-bridge flyback converter employing a parallel–series transformer. *IEEE Trans. Ind. Electron.* **2012**, *60*, 3115–3125.
17. Lee, S.; Yi, J.; Kim, W.; Cho, B.H. A parallel-series connected four-transformer half bridge DC–DC converter for electric vehicle application. In *Proceedings of the 2013 IEEE ECCE Asia Downunder, Melbourne, VIC, Australia, 3–6 June 2013*; IEEE: New York, NY, USA, 2013; pp. 711–715.
18. Lin, B.R.; Wu, S.F. ZVS resonant converter with series-connected transformers. *IEEE Trans. Ind. Electron.* **2010**, *58*, 3547–3554. [\[CrossRef\]](#)
19. Shen, Y.; Zhao, W.; Chen, Z.; Cai, C. Full-bridge LLC resonant converter with series-parallel connected transformers for electric vehicle on-board charger. *IEEE Access* **2018**, *6*, 13490–13500. [\[CrossRef\]](#)
20. Fei, C.; Lee, F.C.; Li, Q. High-efficiency high-power-density LLC converter with an integrated planar matrix transformer for high-output current applications. *IEEE Trans. Ind. Electron.* **2017**, *64*, 9072–9082. [\[CrossRef\]](#)
21. Mu, M.; Lee, F.C. Design and optimization of a 380–12 V high-frequency, high-current LLC converter with GaN devices and planar matrix transformers. *IEEE J. Emerg. Sel. Top. Power Electron.* **2016**, *4*, 854–862.
22. Mahdizadeh, A.H.; Afjei, E. LLC Resonant Converter Utilizing Parallel-Series Transformers Connection. In *Proceedings of the 2019 International Power System Conference (PSC), Tehran, Iran, 9–11 December 2019*; IEEE: New York, NY, USA, 2019; pp. 472–477.
23. Meneses, D.; Garcia, O.; Alou, P.; Oliver, J.A.; Prieto, R.; Cobos, J.A. Forward micro-inverter with primary-parallel secondary-series multicore transformer. In *Proceedings of the 2014 IEEE Applied Power Electronics Conference and Exposition-APEC 2014, Fort Worth, TX, USA, 16–20 March 2014*; IEEE: New York, NY, USA, 2014; pp. 2965–2971.
24. Lo, Y.K.; Lin, J.Y. Active-clamping ZVS flyback converter employing two transformers. *IEEE Trans. Power Electron.* **2007**, *22*, 2416–2423. [\[CrossRef\]](#)